

# Sonochemical Synthesis of Highly Luminescent Zinc Oxide Nanoparticles Doped with Magnesium(II)\*\*

Huan-Ming Xiong,\* Dmitry G. Shchukin, Helmuth Möhwald, Yang Xu, and Yong-Yao Xia

Zinc oxide nanomaterials have shown great potential for use in ultraviolet laser devices<sup>[1]</sup> and biomedical labels<sup>[2]</sup> as they are nontoxic and cheap photoluminescent semiconductors. Since the band gap of ZnO is 3.37 eV at room temperature, which is much higher than that of the typical quantum dots CdSe (1.7 eV) and CdTe (1.5 eV),<sup>[3]</sup> the construction of ZnO nanoparticles with strong and stable visible emission is always a challenge for chemists. In most cases, the photoluminescence (PL) of ZnO nanoparticles has two components. One is the typical exciton emission, that is, photogenerated electrons recombine with the holes at the valence band emitting UV light. The other is defect-based emission in the visible spectrum, the corresponding mechanism of which is not fully understood yet.<sup>[4]</sup> In general, highly crystalline ZnO nanoparticles obtained by pyrolysis or solvothermal synthesis are good UV emitters, but their visible emission is very weak.<sup>[5]</sup> On the contrary, ZnO nanoparticles with plenty of defects prepared through simple sol-gel methods at about room temperature exhibit strong visible fluorescence.<sup>[6]</sup>

A typical sol-gel route to produce ZnO nanoparticles is the hydrolysis of a zinc salt in alcohol.<sup>[7]</sup> After the nucleation stage, the ZnO emission exhibits a continuous red-shift and its quantum yield (QY) decreases gradually.<sup>[8]</sup> Protective organic groups must be grafted on the ZnO surface to prevent further growth and aggregation.<sup>[9]</sup> However, by using this method, one can stabilize ZnO only during its growth, and its luminescence properties can be influenced by the surroundings. As a result, the PL of ligand-grafted ZnO nanoparticles is easily reduced under experimental conditions such as heating, drying, dilution, dialysis, ligand exchange, and phase transfer, which break the nanoparticle-ligand equilibrium. In order to internally adjust the PL of ZnO, Mg<sup>2+</sup>, Cd<sup>2+</sup>, Fe<sup>2+</sup>, and Mn<sup>2+</sup> ions have been doped into ZnO nanocrystals,<sup>[10]</sup> which resulted in the ZnO band gap being successfully adjusted. Unfortunately, the doping processes required a high temperature and the resulting alloy nanocrystals were mainly UV emitters. To our knowledge, Mg<sup>2+</sup> or other metal ion

doped ZnO nanoparticles with strong visible emission have not been reported to date.

Herein, we report the intercalation of Mg<sup>2+</sup> ions into the lattice of ZnO nanoparticles by using strong sonication of 1000 W cm<sup>-2</sup> amplitude at 20 kHz. Sonochemical synthesis is essentially different from the other conventional methods because the ultrasonic wave produces cavitation in the liquid and initiates rapid chemical reactions in cavitation bubbles under extreme conditions.<sup>[11]</sup> The transient collapse of the cavitation bubbles leads to temperatures of about 5000 K, pressures of about 1000 atm, and heating or cooling rates above 10<sup>10</sup> K s<sup>-1</sup> in the cavitation zone, but, for the reaction solution as a whole, the temperature is only moderately elevated and the pressure remains at atmospheric level. Under ultrasonic treatment, Mg<sup>2+</sup> ions quickly diffuse into the ZnO lattice, while ZnO crystallization at high temperature is avoided. As a result, the band gap of the nanoparticles is tuned from 3.4 eV to 3.8 eV and their emission wavelength changes from yellow (ca. 540 nm) to blue (ca. 470 nm). These magnesium(II)-doped ZnO nanoparticles exhibit intense PL with a QY of above 60%, which is four times higher than that of prototypical ZnO nanoparticles. X-ray and electron diffraction results show that the incorporation of Mg<sup>2+</sup> ions decreases the crystallinity of the ZnO without the formation of MgO and Mg(OH)<sub>2</sub> phases. IR analysis confirms the presence of Mg-O-Zn bonds in the final product, which indicates that Mg<sup>2+</sup> ions are doped into ZnO nanoparticles to form new amorphous Mg/ZnO alloys.

In the classical sol-gel synthesis of ZnO quantum dots,<sup>[7b]</sup> Zn(OAc)<sub>2</sub>·2H<sub>2</sub>O is dissolved in absolute ethanol, heated at reflux for 3 h, and then reacted with LiOH·H<sub>2</sub>O at room temperature. The products are green-emitting ZnO nanoparticles with acetate surface groups, and their QY is usually below 10%. Precipitation by addition of a “nonsolvent” is used to purify the ZnO nanoparticles,<sup>[12]</sup> but the purified colloids are yellow-emitting because the acetate groups are so small that they cannot hinder particle agglomeration caused by precipitation. Drying such colloids produces powders with only weak yellow emission.<sup>[9b]</sup> However, by employing a new strategy, we successfully produce the acetate-protected ZnO nanoparticles that possess stable emission from blue to yellow both in sols and as powders. This strategy includes three unreported modifications on the classical sol-gel method. Firstly, tetraethylene glycol (TEG, boiling point 314 °C) was chosen as the reaction medium. Secondly, Zn(OAc)<sub>2</sub>·2H<sub>2</sub>O and LiOH·H<sub>2</sub>O are dissolved together in TEG at room temperature, without any heating. Thirdly, ultrasonication is employed to dope Mg<sup>2+</sup> ions into the ZnO nanoparticles.

The normalized PL spectra of the purified Mg/ZnO colloids in ethanol are compared in Figure 1. No samples

[\*] Prof. H. M. Xiong, Y. Xu, Prof. Y. Y. Xia  
Department of Chemistry and Shanghai Key Laboratory of  
Molecular Catalysis and Innovative Materials, Fudan University  
200433 Shanghai (P.R. China)  
E-mail: hmxiong@fudan.edu.cn

Dr. D. G. Shchukin, Prof. H. Möhwald  
Max-Planck Institute of Colloids and Interfaces  
14424 Potsdam (Germany)

[\*\*] This work was supported by an Alexander von Humboldt Research  
Fellowship in Germany and the National Natural Science Founda-  
tion of China (grant no. 20873029).

Supporting information for this article is available on the WWW  
under <http://dx.doi.org/10.1002/anie.200805590>.

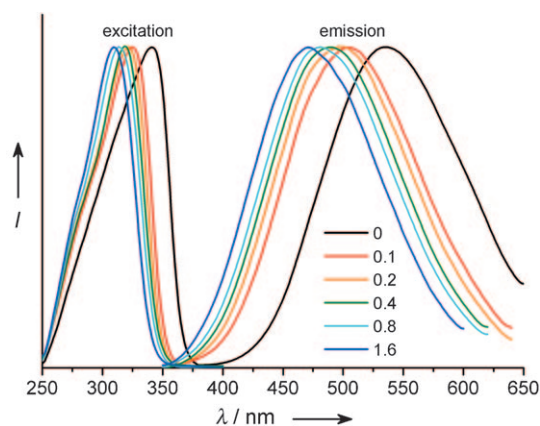


**Figure 1.** Photoluminescence excitation and emission spectra of dilute ethanolic solutions of the purified Mg/ZnO nanoparticles with different Mg/Zn ratios. For each sample, the excitation spectrum was obtained by setting the observation wavelength at its emission peak, while the respective emission spectrum was measured by setting the irradiation wavelength at its excitation peak.

show the exciton emission at around 370 nm. To study the effect of  $\text{Mg}^{2+}$  ions on the properties of the Mg/ZnO nanoparticles, the synthetic molar ratios of Mg/Zn (designated as  $B$ ) were varied from 0 to 1.6. When  $B = 0$ , sonication induces a color shift of the ZnO PL from green to yellow, which is typical for ZnO nanoparticles grown and aggregated by heating.<sup>[9]</sup> XRD and UV/Vis data confirm that the ZnO nanoparticles grow from 3.7 nm to about 5 nm. In contrast, although the solution temperature increases above 180 °C after sonication, the PL spectra for those ZnO samples with  $\text{Mg}^{2+}$  ions are significantly blue-shifted, which increases with higher  $B$  values. After purification by precipitation, the QY of the resulting ethanol solution increases from 16% ( $B = 0$ ) to 66% ( $B = 0.8$ ), and the dried nanoparticles also show very strong fluorescence (see Figure 2), with a QY that was not expected for simple acetate-protected ZnO nanoparticles.

Inductively coupled plasma (ICP) measurements show that actual molar ratios in the final products are slightly lower than the  $B$  values (Table 1). When the  $B$  value increases from 0 to 1.6, the approximate UV/Vis absorption onsets of the Mg/ZnO colloids shift from 370 nm to 330 nm. The average diameter of the ZnO nanoparticles can be calculated on the basis of absorption data by using Meulenkamp's method,<sup>[12a]</sup> these results are in accordance with those obtained by employing the Debye–Scherer formula.<sup>[12b]</sup> When  $B = 0$ , the particle diameter is increased from 3.7 nm to about 5 nm by sonication. However, the particle diameter decreases from 3.1 nm ( $B = 0.1$ ) to 2.5 nm ( $B = 1.6$ ) in presence of  $\text{Mg}(\text{OAc})_2$ . Parallel experiments without sonication show that when adding  $\text{Mg}(\text{OAc})_2$  into the equilibrium system  $\text{Zn}(\text{OAc})_2 + 2\text{LiOH} \rightleftharpoons \text{ZnO} + 2\text{LiOAc} + \text{H}_2\text{O}$ ,  $\text{Mg}(\text{OAc})_2$  reacts with LiOH to form hydrated MgO. A higher concentration of the  $\text{Mg}^{2+}$  ions in solution leads to a smaller size of the ZnO nanoparticles, thus their PL spectra are blue-shifted. Since hydrated MgO can protect ZnO nanoparticles, a small addition of  $\text{Mg}(\text{OAc})_2$  increases the PL intensity. The excess of  $\text{Mg}(\text{OAc})_2$  ( $B = 1.6$ ) consumes ZnO nanoparticles, thus decreasing the emission intensity. These phenomena are

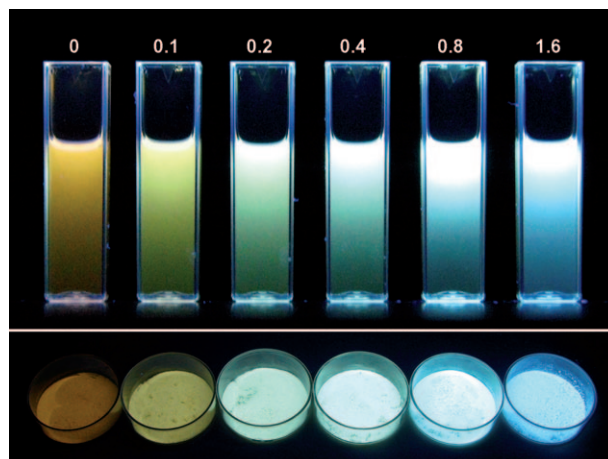


**Figure 2.** Images of ethanolic solutions (upper) and dried powder (lower) of the Mg/ZnO nanoparticles with different Mg/Zn ratios under UV light.

**Table 1:** Comparison between Mg/ZnO nanoparticles with different Mg/Zn ratios ( $B$ ).

$B$	ICP data final ratios	Size <sup>[a]</sup> [nm]	Size <sup>[b]</sup> [nm]	Band gap <sup>[c]</sup> [eV]	Emission maximum [nm]	Quantum yield
0	0	3.7	3.7	3.50	509	16%
0	0	5.1	4.8	3.41	538	21%
0.1	0.057	3.1	3.1	3.63	505	34%
0.2	0.17	3.0	2.9	3.68	496	45%
0.4	0.35	2.9	2.8	3.71	490	58%
0.8	0.71	2.7	2.7	3.75	481	66%
1.6	1.44	2.5	2.5	3.82	470	61%

[a] Measured by using XRD. The average particle size was evaluated by using the Debye–Scherer formula  $d = 0.89\lambda / (\beta \cos\theta)$ , where  $d$  represents the average diameter of the particles,  $\lambda$  the X-ray wavelength ( $\text{Cu}_{\text{K}\alpha}$ , 1.5418 Å),  $\theta$  the Bragg diffraction angle (half of the measured diffraction angle), and  $\beta$  the peak width in radians at half-height. [b] Measured by using UV/Vis. Meulenkamp's empirical formula is  $1240/\lambda_{1/2} = a + b/D^2 - c/D$ , where  $\lambda_{1/2}$  is the wavelength at which the absorption is half of that at the excitonic peak (or shoulder). When the ZnO diameter  $D$  is within the range 2.5–6.5 nm,  $a$ ,  $b$ , and  $c$  are parameters. [c] Measured by using UV/Vis.

observed for both sonicated and nonsonicated samples. However, the sonicated samples exhibit much stronger PL enhancement and wider wavelength variation, which suggests that they have different structures.

A widely accepted model assumes that ZnO visible emission arises from the transition of shallowly trapped electrons to the deeply trapped holes.<sup>[4a,b]</sup> The photogenerated electrons are shallowly trapped by ZnO surface defects (probably  $\text{Zn}^{2+}$ ), while the photogenerated holes are first trapped by ZnO surface defects (probably  $\text{O}^{2-}$ ) and then the

holes tunnel back into the particle interior (the holes are deeply trapped by oxygen vacancies) to form emission centers. Recent results<sup>[5,9]</sup> suggest that visible ZnO emission was dependent on its surface defects, while its internal crystalline phase was responsible for the UV emission. Reduction of the ZnO particle size has two effects: one is the increase of the relative concentration of surface defects compared to bulk lattice sites, which thus increases the probability of trapping electrons or holes on the ZnO surface; the other is the reduction of the distance between shallow traps and deep traps, which thus facilitates electron or hole transfer. Hence, the reduction of the ZnO particle size always resulted in an improvement of the QY. For example, the QY of 20% for acetate-protected ZnO nanoparticles of about 1.4 nm in 2-propanol decreased gradually to 12% as the ZnO diameter grew to about 2 nm.<sup>[8b]</sup> However, the sonicated sample ( $B=0$ ) has a higher QY than the nonsonicated sample ( $B=0$ ) although it is the former that has the larger size (Table 1). This result can be interpreted by ultrasonic effects on nanoparticle growth, that is, the sonicated sample has a disordered structure compared to its counterpart grown under homogeneous mild conditions, which is because sonication provides a constantly changing environment for particle growth. Therefore, increasing the ZnO internal defect concentration is a more effective method of improving the QY than controlling only the ZnO particle size.

The TEM images in Figure 3 illustrate that the ZnO nanoparticle ( $B=0$ ) diameters are about 5 nm and those of the Mg/ZnO alloys ( $B=0.1, 0.2,$  and  $0.4$ ) are about 3 nm, which are in agreement with the diameters calculated from the UV/Vis data and XRD patterns. However, for the other samples with a higher content of  $Mg^{2+}$  ions ( $B=0.8$  and  $1.6$ ), the nanoparticles are so small and amorphous that they can not be seen clearly. Their XRD and electron diffraction patterns indicate that the crystallinity becomes weaker as the  $B$  value increases. For all samples, only the ZnO wurtzite phase can be identified in the electron diffraction and XRD patterns. Therefore,  $Mg^{2+}$  ions could form either amorphous hydrates that show no signals under TEM and XRD measurements, or be doped into ZnO nanoparticles to result in amorphous  $Mg_xZn_{1-x}O$  alloys.<sup>[10]</sup> Bang and co-workers<sup>[13]</sup> found that deposition of

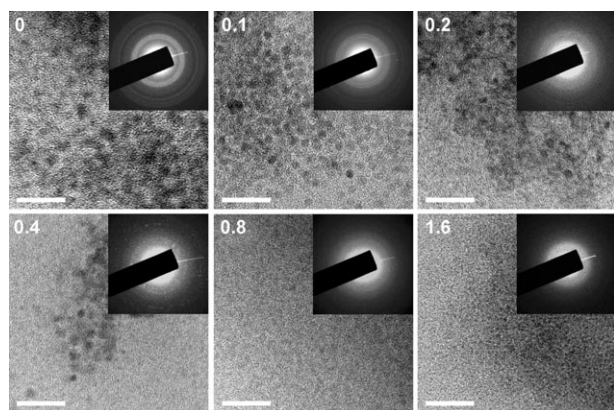


**Figure 3.** TEM images and electron diffraction patterns of the Mg/ZnO nanoparticles with different Mg/Zn ratios. Scale bar: 20 nm.

MgO (band gap 7.8 eV) onto the ZnO nanoparticles could enhance green ZnO emission, which was ascribed to the suppression of nonradiative recombination on the ZnO surface. Rakshit and Vasudevan<sup>[14]</sup> prepared ZnO/MgO core-shell nanoparticles with a QY of 20%. When these nanoparticles were capped by  $\beta$ -cyclodextrins, they could be dissolved in water but the QY of the solution was only 7%. These ZnO/MgO particles derived from sol-gel routes exhibited no signals for the MgO phase in both XRD and TEM measurements. Crystalline MgO is generally prepared by calcination of amorphous hydrated MgO obtained from the sol-gel method.<sup>[15]</sup> Hydrated MgO is able to protect ZnO, but the resulting ZnO/MgO species exists as neither crystalline ZnO@MgO core-shell nanoparticles nor magnesium(II)-doped ZnO nanocrystals.

IR spectroscopy was employed to find the exact location of the  $Mg^{2+}$  ions in the Mg/ZnO nanoparticles. If the  $Mg^{2+}$  ions are outside the ZnO, the MgO hydrates should exhibit their characteristic Mg-OH IR vibrations<sup>[16]</sup> at about  $3700\text{ cm}^{-1}$ ; both this band and the broad OH absorption at about  $3400\text{ cm}^{-1}$  should increase with the  $B$  value. Otherwise, Mg-O-Zn bonds should appear, which will influence the original Zn-O vibration. For both micro-sized and nano-sized commercial MgO, the IR absorption at about  $3700\text{ cm}^{-1}$  is characteristic for Mg-OH vibrations (see Figure 4 and Figure S7 in the Supporting Information).<sup>[15]</sup> Hence, if the final products are ZnO nanoparticles with hydrated MgO shells, there should be strong IR peaks at about  $3700\text{ cm}^{-1}$ , the intensity of which, as well as that of the OH absorption at around  $3400\text{ cm}^{-1}$ , should increase with the  $B$  value. However, no peaks at around  $3700\text{ cm}^{-1}$  are detected in the Mg/ZnO samples, and the OH absorption at around  $3400\text{ cm}^{-1}$  remains unchanged. Therefore, the IR analysis rules out the presence of hydrated MgO in the final products. The most important information in the IR spectrum is found in the

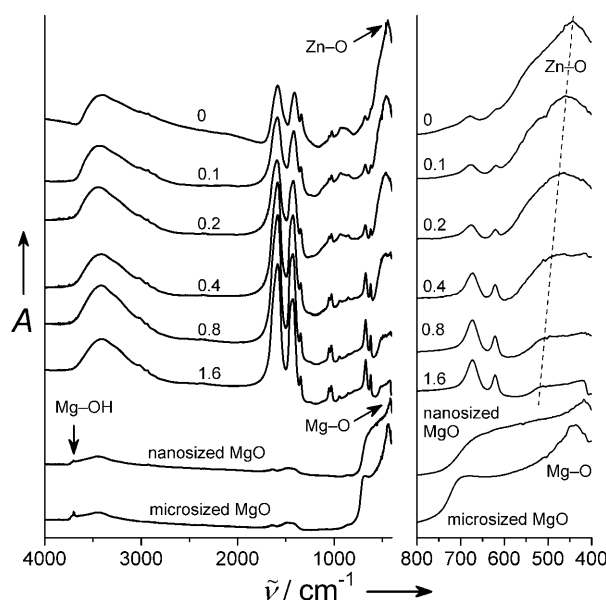


**Figure 4.** FTIR absorbance spectra of the Mg/ZnO powder with different Mg/Zn ratios and the pure MgO powder (nanosized and micro-sized; Aldrich).



region below  $800\text{ cm}^{-1}$ , which is not affected by the water content and illustrates the presence of internal metal–oxygen interactions. The Mg–O vibrations for the nanosized MgO exhibit a broad absorption band with a maximum at  $418\text{ cm}^{-1}$ , while this IR band shifts to higher frequency with its peak at  $450\text{ cm}^{-1}$  for the microsized MgO (Figure 4, right). In addition, for the nanosized ZnO ( $B = 0$ ), the Zn–O vibration is located at  $443\text{ cm}^{-1}$ . The Zn–O absorption band shifts to higher frequency and its intensity decreases gradually as the  $B$  value increases. Such a blue-shift is ascribed to doping with the smaller  $\text{Mg}^{2+}$  ions, which strengthens the metal–oxygen bonds. Moreover, the appearance of an IR absorption at around  $420\text{ cm}^{-1}$  for the samples with  $B = 0.4, 0.8,$  and  $1.6$  also indicates the formation of Mg–O–Zn bonds. The decrease in intensity of the entire metal–oxygen band is due to the decrease of both the degree of crystallinity and the particle size. The reduction in size of the nanoparticles by the addition of  $\text{Mg}^{2+}$  ions renders the increase of both the particle surface area and the acetate group proportion in the whole samples. Thus, IR bands in the region of  $1700\text{--}600\text{ cm}^{-1}$ , which correspond to C=O, C–O, and C–H vibrations respectively, increase with the  $B$  value.<sup>[12b]</sup> For example, the decrease of the particle radius by a factor of two (from  $B = 0$  to  $B = 1.6$ ) would cause an increase of the surface area by a factor of four, which corresponds roughly to the increase of the IR intensity. According to the above analyses, the IR data prove that  $\text{Mg}^{2+}$  ions are doped into the ZnO lattice to form amorphous Mg/ZnO species.

In summary,  $\text{Mg}^{2+}$  ions are intercalated into ZnO nanoparticles by strong sonication to form amorphous Mg/ZnO nanoparticles, which exhibit highly efficient PL both in colloidal dispersions and in the solid state. Increasing the proportion of  $\text{Mg}^{2+}$  ions enables the tuning of the emission wavelength from yellow to blue. The luminescence properties of the nanoparticles are very stable during heating, drying, and storage, which indicates that their luminescence is independent of the surrounding environment but relies on their internal structure. In this work, we have made progress in controlling ZnO luminescence by adjusting the internal defects of ZnO quantum dots.

## Experimental Section

All chemicals were used as received from Sigma–Aldrich.  $\text{Zn}(\text{OAc})_2 \cdot 2\text{H}_2\text{O}$  (0.002 mol) and  $\text{LiOH} \cdot \text{H}_2\text{O}$  powder (0.003 mol) were dissolved in TEG (40 mL) and stirred at room temperature until the solution became luminescent.  $\text{Mg}(\text{OAc})_2 \cdot 4\text{H}_2\text{O}$  powder was then added to the solution according to the molar ratio  $B = \text{Mg}/\text{Zn}$ , followed by sonication at  $1000\text{ W cm}^{-2}$  20 kHz using a titanium horn in a UIP 1000 hd Hielscher ultrasonic processor. Each solution was sonicated continuously for 2 min, and its final temperature was  $(180 \pm 10)^\circ\text{C}$ . The solution was immediately cooled in an ice-water bath. Parallel experiments were conducted with the same reactants but without sonication treatment. All samples were kept at room temperature for one day before PL measurements. An excess of ethyl acetate was added into each TEG solution as nonsolvent to precipitate the nanoparticles, which were isolated by centrifugation, the precipitate was then redispersed in a small amount of absolute ethanol. Such precipitation–redispersion treatment was repeated in order to purify the products thoroughly, and the final colloids in ethanol were used for characterization. TEM images were taken with

a JEM-2010 transmission electron microscope operating at 200 kV, UV/Vis absorption spectra were obtained with an Agilent 8453 ultraviolet–visible spectrometer and PL spectra were recorded on a Horiba Jobin Yvon fluoromax-4 spectrofluorometer. A solution of Rhodamine 6G in ethanol (QY = 95 %) was used as the reference to evaluate the QY of each product. These ethanol solutions were vaporized and dried in an oven at  $100^\circ\text{C}$ . The obtained powder was scanned by a Bruker D8 X-ray powder diffractometer and a Bruker Equinox 55/S Fourier transform infrared spectrometer. To determine the Zn/Mg molar ratio in each sample, the powder was dissolved in an aqueous solution of HCl and tested with an Agilent 7500 CS inductively coupled plasma mass spectrometer.

Received: November 15, 2008

Revised: February 9, 2009

Published online: March 6, 2009

**Keywords:** doping · luminescence · nanostructures · nanotechnology · ultrasonic synthesis

- [1] a) M. H. Huang, S. Mao, H. Feick, H. Q. Yan, Y. Y. Wu, H. Kind, E. Weber, R. Russo, P. D. Yang, *Science* **2001**, *292*, 1897; b) Z. R. Dai, Z. W. Pan, Z. L. Wang, *Adv. Funct. Mater.* **2003**, *13*, 9; c) Z. K. Tang, G. K. L. Wong, P. Yu, M. Kawasaki, A. Ohtomo, H. Koinuma, Y. Segawa, *Appl. Phys. Lett.* **1998**, *72*, 3270.
- [2] a) H. M. Xiong, Y. Xu, Q. G. Ren, Y. Y. Xia, *J. Am. Chem. Soc.* **2008**, *130*, 7522; b) Y. F. Liu, Y. B. Zhang, S. P. Wang, C. Pope, W. Chen, *Appl. Phys. Lett.* **2008**, *92*, 143901.
- [3] a) H. Weller, *Angew. Chem.* **1993**, *105*, 43; *Angew. Chem. Int. Ed. Engl.* **1993**, *32*, 41; b) X. Peng, U. Manna, W. Yang, J. Wickham, E. Scher, A. Kadavanich, A. P. Alivisatos, *Nature* **2000**, *404*, 59; c) H. Zhang, D. Wang, B. Yang, H. Möhwald, *J. Am. Chem. Soc.* **2006**, *128*, 10171; d) T. Trindade, P. O'Brien, N. L. Pickett, *Chem. Mater.* **2001**, *13*, 3843.
- [4] a) A. van Dijken, E. A. Meulenkaamp, D. Vanmaekelbergh, A. Meijerink, *J. Phys. Chem. B* **2000**, *104*, 1715; b) A. van Dijken, E. A. Meulenkaamp, D. Vanmaekelbergh, A. Meijerink, *J. Lumin.* **2000**, *90*, 123; c) M. L. Kahn, T. Cardinal, B. Bousquet, M. Monge, V. Jubera, B. Chaudret, *ChemPhysChem* **2006**, *7*, 2392; d) H. M. Xiong, D. P. Xie, X. Y. Guan, Y. J. Tan, Y. Y. Xia, *J. Mater. Chem.* **2007**, *17*, 2490.
- [5] a) T. Andelman, Y. Gong, M. Polking, M. Yin, I. Kuskovsky, G. Neumark, S. O'Brien, *J. Phys. Chem. B* **2005**, *109*, 14314; b) Y. F. Chen, M. Kim, G. Lian, M. B. Johnson, X. G. Peng, *J. Am. Chem. Soc.* **2005**, *127*, 13331; c) Y. S. Wang, P. J. Thomas, P. O'Brien, *J. Phys. Chem. B* **2006**, *110*, 4099.
- [6] a) M. Abdullah, I. W. Lenggoro, K. Okuyama, F. G. Shi, *J. Phys. Chem. B* **2003**, *107*, 1957; b) H. M. Xiong, Z. D. Wang, Y. Y. Xia, *Adv. Mater.* **2006**, *18*, 748; c) Y. S. Fu, X. W. Du, S. A. Kulinich, J. S. Qiu, W. J. Qin, R. Li, J. Sun, J. Liu, *J. Am. Chem. Soc.* **2007**, *129*, 16029.
- [7] a) D. W. Bahnemann, C. Kromann, M. R. Hoffmann, *J. Phys. Chem.* **1987**, *91*, 3789; b) L. Spanhel, M. A. Anderson, *J. Am. Chem. Soc.* **1991**, *113*, 2826.
- [8] a) L. Spanhel, *J. Sol-Gel Sci. Technol.* **2006**, *39*, 7; b) A. van Dijken, J. Makkinje, A. Meijerink, *J. Lumin.* **2001**, *92*, 323.
- [9] a) H. M. Xiong, D. P. Liu, Y. Y. Xia, J. S. Chen, *Chem. Mater.* **2005**, *17*, 3062; b) H. M. Xiong, Z. D. Wang, D. P. Liu, J. S. Chen, Y. G. Wang, Y. Y. Xia, *Adv. Funct. Mater.* **2005**, *15*, 1751; c) D. P. Liu, G. D. Li, Y. Su, J. S. Chen, *Angew. Chem.* **2006**, *118*, 7530; *Angew. Chem. Int. Ed.* **2006**, *45*, 7370.
- [10] a) Y. S. Wang, P. J. Thomas, P. O'Brien, *J. Phys. Chem. B* **2006**, *110*, 21412; b) Y. Kim, R. Seshadri, *Inorg. Chem.* **2008**, *47*, 8437; c) J. Bian, Y. Luo, J. Sun, H. Liang, W. Liu, L. Hu, *J. Mater. Sci.* **2007**, *42*, 8461; d) F. K. Shan, B. I. Kim, G. X. Liu, Z. F. Liu, J. Y. Sohn, W. J. Lee, B. C. Shin, Y. S. Yu, *J. Appl. Phys.* **2004**, *95*, 4772.

- [11] a) K. S. Suslick, *Science* **1990**, *247*, 1439; b) K. S. Suslick, G. J. Price, *Annu. Rev. Mater. Sci.* **1999**, *29*, 295; c) D. G. Shchukin, H. Möhwald, *Phys. Chem. Chem. Phys.* **2006**, *8*, 3496; d) D. G. Shchukin, H. Möhwald, *Small* **2007**, *3*, 926.
- [12] a) E. A. Meulenkaamp, *J. Phys. Chem. B* **1998**, *102*, 5566; b) H. M. Xiong, X. Zhao, J. S. Chen, *J. Phys. Chem. B* **2001**, *105*, 10169.
- [13] J. Bang, H. Yang, P. H. Holloway, *Nanotechnology* **2006**, *17*, 973.
- [14] a) S. Rakshit, S. Vasudevan, *J. Phys. Chem. C* **2008**, *112*, 4531; b) S. Rakshit, S. Vasudevan, *ACS Nano* **2008**, *2*, 1473.
- [15] a) R. Wahab, S. G. Ansari, M. A. Dar, Y. S. Kim, H. S. Shin, *Mater. Sci. Forum* **2007**, 558–559, 983; b) V. M. Boddu, D. S. Viswanath, S. W. Maloney, *J. Am. Ceram. Soc.* **2008**, *91*, 1718.
- [16] a) W. Wang, X. Qiao, J. Chen, *J. Am. Ceram. Soc.* **2008**, *91*, 1697; b) A. Kumar, J. Kumar, *Solid State Commun.* **2008**, *147*, 405; c) M. Foster, M. D'Agostino, D. Passno, *Surf. Sci.* **2005**, *590*, 31; d) C. Chizallet, G. Costentin, M. Che, F. Delbecq, P. Sautet, *J. Am. Chem. Soc.* **2007**, *129*, 6442.
-